Direct measurement of the electrostatic image force of a levitated charged nanoparticle close to a surface

George Winstone,[1,2] Robert Bennett,[3] Markus Rademacher,[1] Muddassar Rashid,[1] Stefan Buhmann,[3,4] and Hendrik Ulbricht[1,*]

[1]*Department of Physics and Astronomy, University of Southampton, Southampton SO17 1BJ, United Kingdom*

[2]*School for Materials Science, Japan Advanced Institute of Science and Technology, Nomi, Ishikawa 923-1211, Japan*

[3]*Institute of Physics, Albert-Ludwigs-University Freiburg, D-79104 Freiburg, Germany*

[4]*Freiburg Institute for Advanced Studies (FRIAS), D-79104 Freiburg, Germany*

(Received 19 March 2018; published 19 November 2018)

We report on optical levitation experiments to probe the interaction of a nanoparticle with a surface in vacuum. The observed interaction-induced effect is a controllable anharmonicity of the particle trapping potential. We reconstruct the Coulomb image charge interaction potential to be in perfect agreement with the experimental data for a particle carrying $Q = -(11 \pm 1)e$ elementary charges and compare the measured electrostatic interaction with the weaker dispersive forces from theory. Our experimental results may open the route for a new surface sensitive scanning probe technique based on the high mechanical sensitivity of levitated nanoparticles.

DOI: 10.1103/PhysRevA.98.053831

I. INTRODUCTION

Weak forces in close proximity to surfaces have important real-world relevance across a range of settings in the nano world, from colloids [1] to nanomechanical devices [2,3] and possibly even protein folding [4–6]. Alongside this, they can also be used for detection of weak long-range forces, such as gravity [3,7–9] and hypothetical interactions aiming to solve the problem of dark energy [10]. There is an assortment of different forces which can contribute to atom-surface interactions. A particle with nonzero net charge near a surface will experience an attractive force via Coulomb interaction with its image. A competing class of effects that persist even for neutral objects arise from correlations between the fluctuations of atomic dipoles that make up two spatially separated bodies; these are dispersion forces. A famous example is the Casimir force [11] between two macroscopic objects, while a related effect for the case where one object is macroscopic and the other is microscopic (atom, molecule, nanosphere, etc.) is known variously as the Casimir-Polder (CP) [12] and the van der Waals force in the case of two microscopic bodies.

A model system in which weak forces at short distances can be experimentally studied consists of two closely spaced objects separated by a variable-width vacuum gap, as depicted in Fig. 1(a). Over the years a variety of experiments of this type have been performed with different physical systems (e.g., torsion pendulums [13], cantilevers, and tip probes [14]) to investigate surface forces. Several experiments that utilize controllable cold atoms have been performed to measure weak forces close to an uncharged surface [15–18]. Charged particles interacting with surfaces have been studied in great detail by trapped atomic ion experiments, as electric field noise related to that particle-surface interaction is a limiting factor in precision experiments with atomic ions and a common problem in ion trapping. Still, the fine details of the different mechanisms that eventually result in the field noise are poorly understood (see, for example, [19] for a review of this field).

Here we report on experiments with a single electrically charged glass nanoparticle optically levitated in close proximity to a neutral silicon surface in vacuum, which allows for direct measurement of electrostatic forces in a distance and sensitivity regime outperforming most existing force microscopies [20]. However, in our experiments we do not currently reach the regime necessary to experimentally resolve dispersion forces such as CP and van der Waals.

II. EXPERIMENTAL METHODS

The experimental configuration used in this study is depicted schematically in Fig. 1(a). A silica nanoparticle is trapped at a variable distance d away from a silicon surface in a tiny light spot focused by a parabolic mirror. The vacuum is low enough that the optically trapped particle is still affected by stochastic background gas collisions, so that the equation of motion for its displacement x is

$$\ddot{x} + \gamma\dot{x} + \Omega x = \frac{F(t)}{m}, \tag{1}$$

where γ describes the damping of the motional degree of freedom of the particle, Ω is the natural frequency of the oscillator, m represents its mass, and $F(t)$ describes the fluctuating forces acting on the particle according to random collisions with background gas particles. The particle's position is not stabilized by any feedback and is allowed to move freely in the trap at different d values. The particle is electrically charged and we later determine that it carries a net charge of 11 elementary charges e. Based on our optical detection of the particle's position we can measure time traces of the particle position with the high interferometric resolution

*h.ulbricht@soton.ac.uk

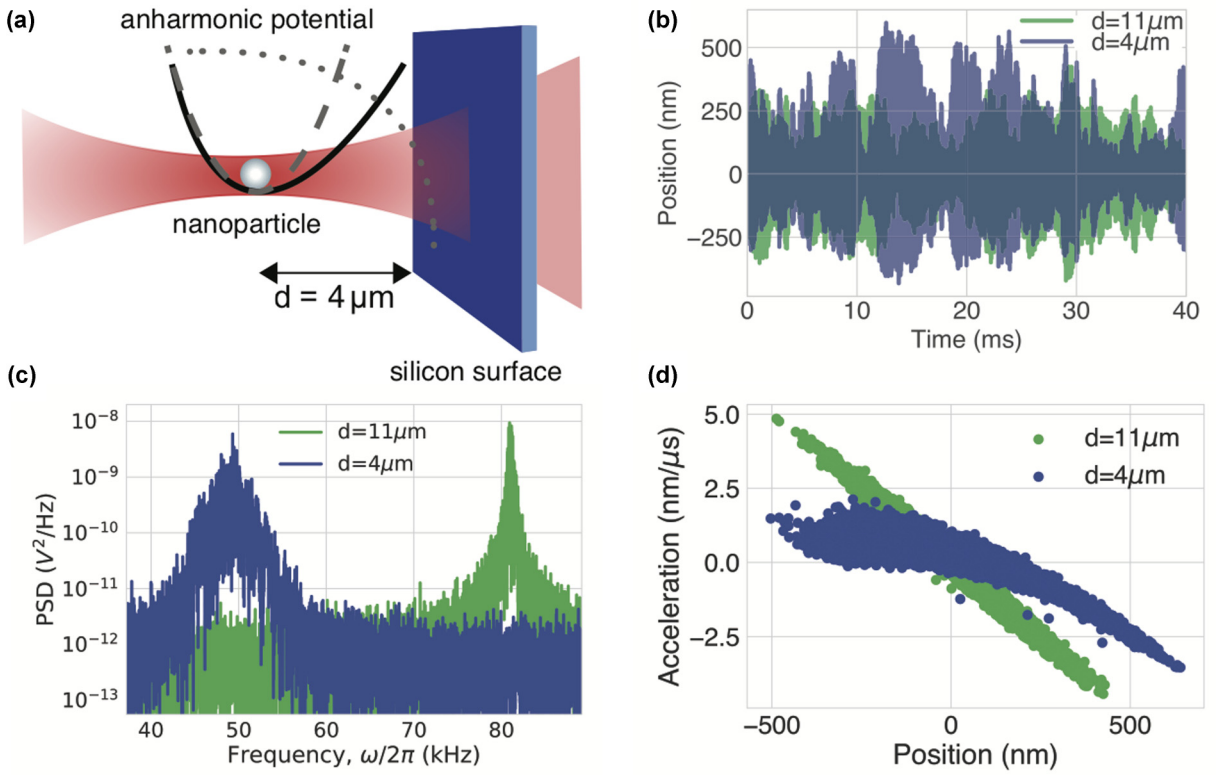

FIG. 1. Particle-surface experiment with a levitated nanosphere. (a) Schematic of the experiment. The particle is optically trapped close to the surface at various distances d. (b) Time trace of the particle position trapped close to and far away from the surface. The amplitude of the oscillation increases when the particle is closer to the surface. (c) Power spectral densities (PSDs) of z motion of the trapped particle at two distances; (d) the related spring functions. The spring function shows a nonlinear shape if the particle is close to the surface.

of 1 pm. Typical time-domain data on the trapped particle are shown in Fig. 1(b), which gives information about the motion of the particle in all three spatial directions. The directions can be disentangled in the frequency domain, so that we are able to concentrate here only on the motion in the z direction, which is normal to the plane of the trapping mirror. The power spectral density (PSD) of the z motion is shown in Fig. 1(c). From such data we can extract the actual shape of the trapping potential, which is harmonic if the only significant trapping potential is the optical one. If the particle is close to the surface the potential becomes anharmonic, which we can directly extract from the data as shown in Fig. 4(b). We then reconstruct the surface potential from these experimental data, which is the basic technique in this paper. We can also extract the so-called spring function (position-acceleration trace) of the motion of the particle as shown in Fig. 1(d). This shows clearly distinguishable behavior for the two cases where the particle is close to and far away from the surface.

A. Experimental setup

We optically trap a dielectric SiO_2 nanosphere in the focus of a high-numerical-aperture (NA = 0.9) parabolic mirror. The nanosphere is positioned a variable distance (4 to 11 μm) away from a surface consisting of a 200-μm-thick, highly n-doped Si(100) wafer with a 300-nm SiO_2 layer on top. The trapping laser wavelengths and power are 1550 nm and 1 W, respectively. All experiments are conducted at a pressure of 10^{-2} mb, while no active cooling of the center-of-mass motion of the particle has been implemented, in order to allow for high oscillation amplitudes of the particle in the trap. The motion of the particle is still both damped and driven by collisions with background gas. However, the effect of the interaction of the particle with the surface already becomes clearly visible and is measurable as it affects the shape of the trap. The experimental setup is shown in Fig. 2 and more

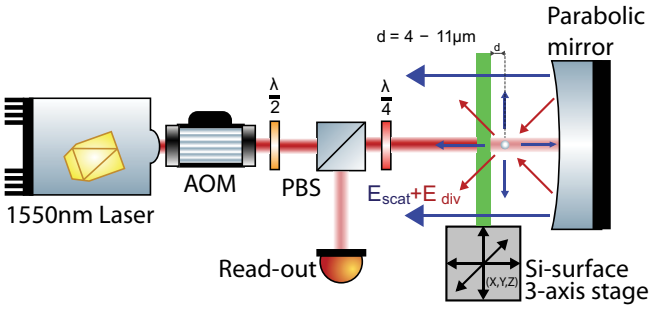

FIG. 2. Experimental setup. The 1550-nm light is focused by reflection off a parabolic mirror to a spot of waist of about 1 μm. The light wave Rayleigh scattered by the particle is superposed on a diverging reference wave, which gives the high position resolution, 1 pm, of the detection. The light is detected by a cooled InGaAs photodiode. The silicon surface, which is optically transparent at the trapping laser wavelength, is mounted on a vacuum-compatible x, y, z stage in order to control the particle-surface distance.

details about optical trapping using parabolic mirrors can be found elsewhere [21,22]. Briefly, a three-axis micrometer stage is used to vary the distance between a 200-μm-thick, highly n-doped, and double-sided polished silicon planar surface (Si wafer), which is transparent at 1550 nm [23], and the optically defined nanoparticle trapping site. The surface is moved in discrete intervals, decreasing the distance to the levitated particle. At each stage position the nanoparticle's motion is recorded by an interferometric detection scheme with a high spatial resolution utilized in previous studies [21,22]. At each stage position, the oscillation of the particle explores a region of several hundred nanometers, with the exact distance being determined by the potential stiffness. This allows us to reconstruct the overall surface potential in piecewise steps.

B. Mass and radius of the trapped particle

In order to extract a potential from time-trace data, we need to know the mass of the particle. To this end we adopt a method from Rondin *et al.* [24], but in one dimension rather than three. The mass is computed by comparing two potentials, namely, the steady-state potential $U_{\rm st}$ and the kinematic potential $U_{\rm kin}$, with the mass m as the only free parameter. The potential $U_{\rm st}$ computed from the steady-state solution of a Langevin equation of a particle at thermodynamic equilibrium with a random background field undergoing a random walk in a potential

$$U_{\rm st} = k_B T \ln(\rho(x)), \tag{2}$$

where $\rho(x)$ represents the position distribution of the trapped particle. The dominant contribution to the damping comes from random kicks of background gas particles with the trapped particle at thermal equilibrium with the environment at 300 K. The potential $U_{\rm kin}$ is extracted experimentally from the time trace of the motion of the particle in the trap according to

$$U_{\rm kin} = \int \mathbf{F}(t)\cdot \mathbf{dx} + C, \tag{3}$$

where C is a constant of integration and $\mathbf{F}(t)$ is the time-dependent net force acting on the particle. The latter is computed by extracting the acceleration from the time trace and then multiplying by the mass. Thus, on the assumption that the particle is at thermal equilibrium, we equate the two potentials, $U_{\rm st} = U_{\rm kin}$, leaving the mass m as the only free fitting parameter. We then extract the radius r from the mass on the assumption that the particle is of a spherical shape. This assumption is supported by the experimental evidence that the motions in different spatial directions are not coupled. A comparison of the two potentials, $U_{\rm stst}$ and $U_{\rm kin}$, is shown in Fig. 3, and we extract a particle radius of $r = 60$ nm (± 5 nm) for the data reported in this paper. The error bar of the particle radius is derived from the fitting error.

III. THEORY

At large distances from the surface, where the surface does not affect the oscillation of the particle, the levitated nanoparticle is trapped optically in the focus of a Gaussian laser beam in the Rayleigh limit. The optical potential is harmonic and given by

$$U_{\rm opt}(x) = \frac{1}{2}kx^2, \tag{4}$$

where x is the spatial displacement of the nanosphere while oscillating, and k is the spring constant. Since the trap at hand originates from the optical gradient force, the spring constant is therefore given by

$$k = \frac{2\alpha P \lambda^2}{\pi \epsilon_0 c w^6}, \tag{5}$$

with α being the polarizability of the nanoparticle, P the incident laser power, w the laser waist at focus, and λ its wavelength. As usual, c is the speed of light and ϵ_0 the permittivity of free space. Here, we only consider the one-dimensional z motion of the particle normal to the surface. More details about the optical trap can be found elsewhere [21].

If the particle is placed near a surface, the optical potential may no longer be the only significant component of the total potential felt by the particle. Since our particle carries a nonzero net charge, the Coulomb interaction will come into play. The Coulomb potential $U_C(d)$ of a particle of charge Q interacting with its image in a dielectric substrate with a layer of thickness L deposited on top can be calculated by following the methods of, for example, Ref. [25]. We find

$$U_C(d) = -\frac{Q^2}{4\pi\epsilon_0}\frac{1}{2}\int_0^\infty d\kappa \frac{R_{01} + R_{12}e^{-2\kappa L}}{1 + R_{01}R_{12}e^{-2\kappa L}} e^{-2\kappa d}, \tag{6}$$

with $R_{01} = (\epsilon_1 - 1)/(\epsilon_1 + 1)$ and $R_{12} = (\epsilon_2 - \epsilon_1)/(\epsilon_2 + \epsilon_1)$, where ϵ_1 and ϵ_2 are the permittivities of the layer and the substrate, respectively. d is the distance between the nanoparticle and the vacuum-layer interface. Close to the surface the particle will explore a total potential $U_{\rm tot}(d)$ defined by

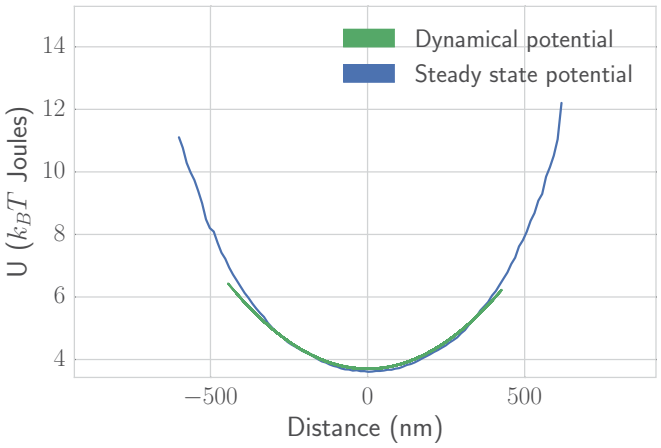

FIG. 3. Mass extraction from potentials. The steady-state, according to Eq. (2), and the kinematic, according to Eq. (3), potentials are fitted to each other, with the mass of the particle as the only free parameter. In this way the mass of the particle is extracted from the measured data directly without assumptions otherwise used. The mass extraction from the potential has been done for large ($d = 11$ μm) distances between the trapped particle and the surface.

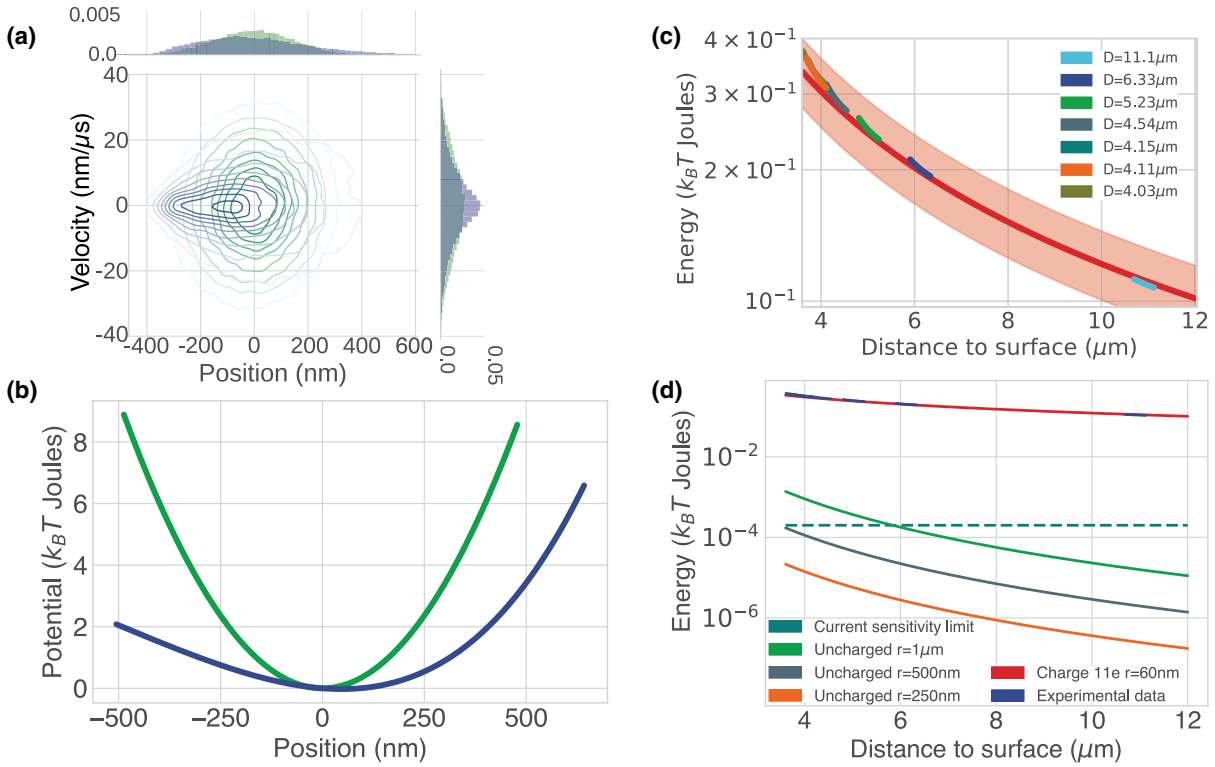

FIG. 4. Nanoparticle surface probe. (a) Dynamics of the particle in a phase-space representation. Contours represent experimental data for positions and velocities of the particle close to (blue) and far away from (green) the surface. Clearly visible is the nonspherical shape in the case of the particle close to the surface, which is due to the interaction with the surface. (b) Reconstructed potential as calculated from experimental data for the particle at various distances. The potential becomes anharmonic if the particle is closer to the surface. (c) Comparison of the experimental data taken at seven distances, with theory according to Eq. (6) shown by the red line. The pink region indicates the same mirror charge interaction with ± 1 elementary charge e. Closer to the surface the best fit with $-11e$ deviates from the experimental data. (d) Comparison of experimental interaction data with different types of potentials, such as the CP potential for particles of different sizes as well as Eq. (6). The dashed horizontal line is the sensitivity limit of the present experiment.

the superposition of the surface interaction potential and the optical potential, $U_{\rm tot}(d) = U_C(d) + U_{\rm opt}(x-d)$. This is an anharmonic potential, with the anharmonicity arising from the surface interaction that is added to the harmonic trapping potential. The degree of anharmonicity can then be used to extract the strength of the surface potential, as detailed in later sections.

Purely for comparison and without making the claim that we can actually measure dispersion forces, we now discuss the effect of CP and van der Waals forces and evaluate their interaction potential. Aside from the Coulomb potential, the nanosphere experiences a dispersion force arising from correlations between the fluctuations of its own atomic dipoles and those in the surface. Here, the nanosphere is far enough away from the surface that it can be considered a point dipole, with the polarizability $\alpha(\omega)$ obtained from the well-known Clausius-Mossotti relation for a sphere of radius R and permittivity $\epsilon(\omega)$:

$$\alpha(\omega) = 4\pi\epsilon_0 R^3 \frac{\epsilon(\omega)-1}{\epsilon(\omega)+2}. \tag{7}$$

In Appendix B, we present numerical results for the CP potential based on (7) for a wide range of distances; however, in order to gain a simple and usable formula we note that the nanosphere-surface distance (4–11 μm) is large compared to the wavelength of any of the dominant transitions in the optical response of either of the materials (70 nm for SiO_2 and 265 nm for Si). Thus, we are in the retarded regime, in which the CP potential has the form [26]

$$U_{\rm CP}(d) = -\frac{C_4}{d^4}, \tag{8}$$

where C_4 is a distance-independent constant defined as [27]

$$C_4 = \frac{3\hbar c\alpha(0)}{64\pi^2\epsilon_0}\int_1^\infty dv\left(\frac{2}{v^2}-\frac{1}{v^4}\right)\frac{\epsilon_1(0)v-\sqrt{\epsilon_1(0)-1+v^2}}{\epsilon_1(0)v+\sqrt{\epsilon_1(0)-1+v^2}}. \tag{9}$$

Using the measured optical data for silicon and silicon dioxide presented in Appendix B tabulated in [26], we find a value of $C_4 = (7.60\times10^{-28}\ \mathrm{J\cdot m})\times R^3$. In the following we compare the data to the trapping and Coulomb potentials U_C and $U_{\rm opt}$.

IV. RESULTS

Our main results for surface-induced potentials are summarized in Fig. 4. First, Fig. 4(a) shows the phase space of the nanosphere's center-of-mass motion far away from the surface (green) and at the closest available position, 4 μm

(blue), before the surface forces overpower the optical forces and the particle gets lost from the trap. The position distribution of the particle is drawn towards the surface and the motion becomes significantly anharmonic.

In the case of a simple, steady-state, differentiable potential, it is therefore possible to reconstruct the potential from the spring functions of the particle's motion at each distance. For experimental data, with and without the surface, we show the reconstructed potentials in Fig. 4(b).

At smaller particle-surface distances d, the trapping potential experiences an increasingly strong perturbation from the surface interaction. Comparing the reconstructed potential with different interaction models shows the best agreement if the nanosphere is taken to carry a charge of $Q = -(11 \pm 1)e$, found from fitting Eq. (6) to the experimental data, as shown in Fig. 4(c). The observed particle net charge is in agreement with typical values in recent experiments with trapped nanoparticles [28,29]. The observed deviation from the model at small distances could be attributable to electrostatic patch effects, since charge and electric dipole patch effects have been shown to contribute in high-sensitivity surface force measurements [30,31].

To estimate the experimental sensitivity, we perturb a suspended nanoparticle with an electric field [29]. This allows us to resolve changes to the potential structure of $2 \times 10^{-4} k_B T$. Encouragingly, applying such a resolution to the distance ranges scanned in this experiment predicts that we should be able to resolve CP forces if the same surface-nanoparticle experiment were to be repeated with a larger particle. We evaluate for this experiment the force sensitivity to be $8 \pm 3 \times 10^{-17}$ N/$\sqrt{\text{Hz}}$, although with an improved signal-to-noise ratio this can reach as low as $\sim 10^{-19}$ N/$\sqrt{\text{Hz}}$ [29], while details of the calculation of force sensitivity are given in Appendix C. This is in contrast to the original atomic force microscope paper [20]. This level of force sensitivity allows for detection of genuine CP interactions for a particle of radius 1 μm, while with the best sensitivity demonstrated in this system to date [29], the study of CP forces with a 300-nm-radius particle appears to be within reach. The sensitivity limit of the present experiment is indicated by the dashed line in Fig. 4(d). Similarly promising is that the lowest particle-surface interaction energies measured here are of the order of 100 μeV, which is the order of magnitude for dispersion forces—much lower energies than those typical for covalent bonds and charge transfer interactions. The spatial resolution of position detection is given by the parabolic mirror trap detection technique and has been demonstrated to reach 200 fm/$\sqrt{\text{Hz}}$ [22]. This makes the spatial resolution of our surface probe technique much finer than the size of the trap, which is of the order of several hundred nanometers.

To probe further the Morse type of the reconstructed anharmonic potential, we plot a histogram of the particle potential energy and again compare the two cases for the particle with and without the surface. The plot is shown in Fig. 5 and the anharmonic potential energy distribution can be well understood by numerically solving the equation of motion; see Appendix A for computational details.

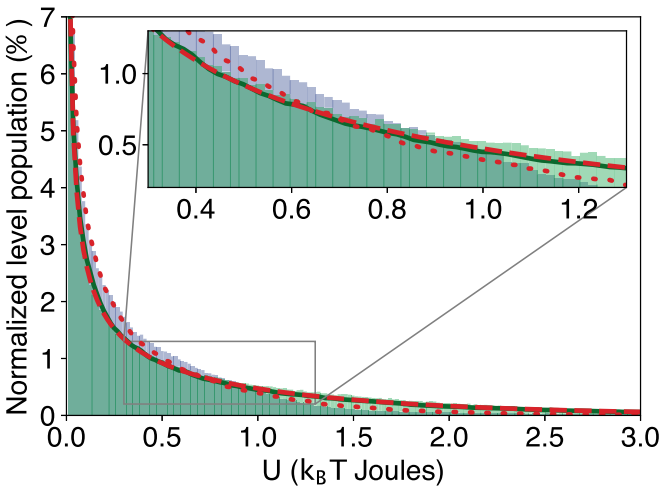

FIG. 5. Energy comparison: harmonic vs anharmonic trap. Normalized histogram of the particle's potential energy for the cases of a harmonic potential (particle far away from the surface; green) and an anharmonic Morse-like potential (particle close to the surface; blue). The former can be found analytically from the normalized result of Eq. (A3) in Appendix A; this is shown as the solid dark-green line. Shown in red are the results of numerical simulation of the particle's motion for harmonic (dashed curve) and anharmonic (dotted curve) potentials with 10 000 different realizations with randomized amplitudes. The Morse-like potential shows a similar behavior in energy level scaling compared to the harmonic case until diverging strongly at a high value of n, which is the expected Morse-like behavior.

A. Potential extraction

1. Spring functions

The potentials governing the particle's motion both close to ($d = 4$ μm) and far away from ($d = 11$ μm) the surface are extracted by integrating the spring functions at each distance between the nanoparticle trap site and the surface. We obtain the spring function for the particle's motion by numerically differentiating the experimentally obtained time trace of the particle's motion with respect to time, as shown in Fig. 6. The frequency of the particle's motion is of the order of 50 kHz, while the sampling frequency of the oscilloscope is 2.5 MHz, giving us about 50 data points per oscillation period and therefore a very good phase-space resolution of the particle's motion. We can then obtain the potential structure experienced kinematically by the particle by numerically integrating the spring function with respect to space.

2. Evaluation of charge Q and distance d from potentials

As the surface-to-particle distance d becomes smaller the potential experienced by the particle is increasingly perturbed by both optical backscatter and the increasing surface forces from the particle. The changes in the optical power, however, are generally symmetrical and can be calibrated against the relative frequency drop of the motion in the x and y axis. To extract the nonsymmetric surface potential from the total potential U_{tot} we consider the total potential as experienced

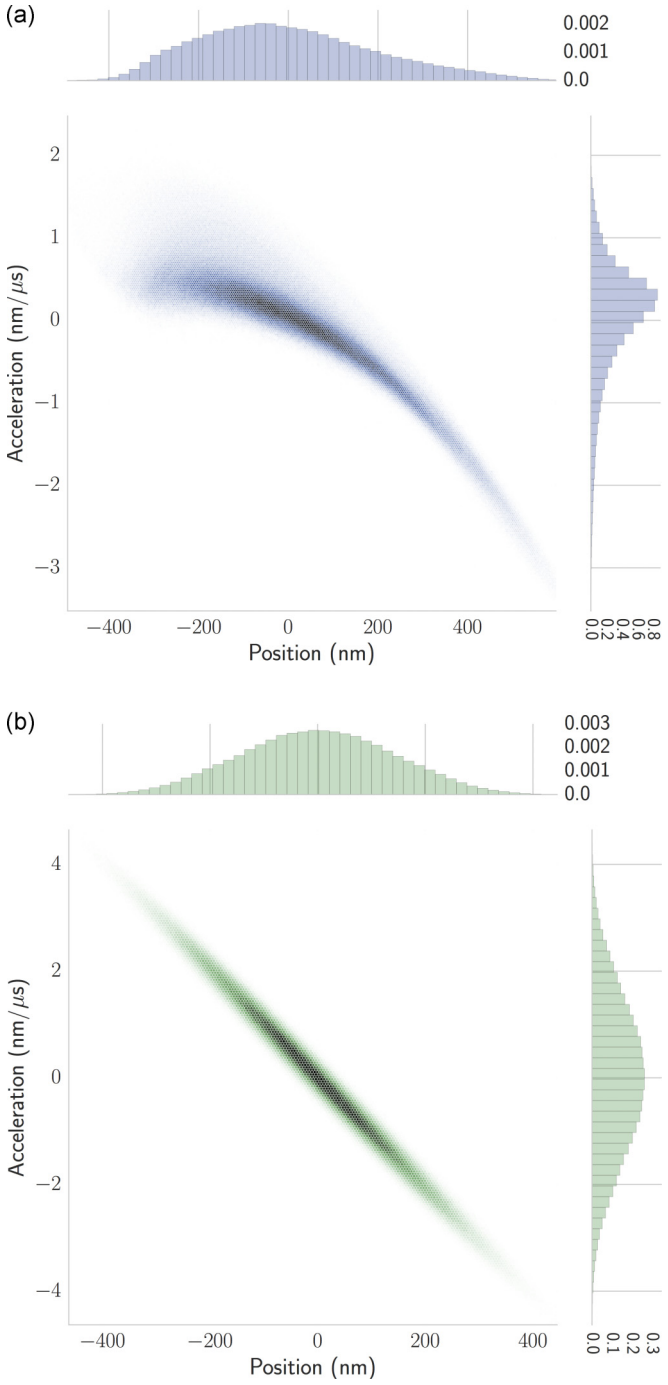

FIG. 6. Acceleration-position spring functions. (a) Spring function for a particle close to the surface. (b) Spring function for a particle far away from the surface. In both panels histograms of the particle's acceleration and position as it moves in the trap are shown at the edges of the main plots.

by the particle and consisting of the harmonic optical trap and the surface interaction $U_C(d)$ shown in Eq. (6):

$$U_{\text{tot}} = \tfrac{1}{2}kx^2 + U_C(d). \tag{10}$$

Here k is the spring constant of the optical trap (for a linear trap), and d is the distance between the center of the optical trap and the silicon surface. The experimentally obtained potential U_{exp} is then used in the equation

$$\tfrac{1}{2}k_{\text{new}}x^2 = U_{\text{exp}} - U_C(d), \tag{11}$$

where k_{new} is a new spring constant, adjusted to fit the parameters Q and d such that the output of the function becomes a symmetrical potential, which is usually a kx^2 function similar to the original, unperturbed, optical trap potential far away from the surface but with a weaker spring function k. Our claim here is that while proximity to the surface does weaken the optical trap, it weakens it in a predictable symmetrical way, and this can be calibrated by the x and y motional peaks. This weakening is not sufficient to explain the anharmonicity experienced by the particle near the surface, whereas a Coulomb image charge model explains it well.

V. DISCUSSION

The use of a nanoparticle as opposed to an atom for force detection has the advantage that the dispersion coefficient C_4 is much larger, giving a stronger force. For example, taking the selection of alkali metals (commonly used in atom-surface experiments) found in [32], one has C_4 coefficients of around 10^{-56} J · m^4, but for a nanosphere of radius 60 nm the corresponding value from Eq. (9) is 1.6×10^{-49} J · m^4—seven orders of magnitude larger. This difference can be qualitatively understood by noting that a hypothetical nanosphere with a radius of 1–2 Å would result in approximately the same C_4 as an atom. The 60-nm sphere in the experiment is around 300 times larger than this, so the cubic scaling of C_4 with the radius means that the nanosphere C_4 is a factor of around 300^6–10^7 larger, as reflected in the calculation above.

Control of the number of electric charges on the particle would be a beneficial addition to the experiment, as it might also allow preparation on demand of an electrically neutral particle. Recently it has been demonstrated experimentally that such control of the number of charges can be done on the single-electric-charge level [28]. Clearly, further understanding of the electric charge distribution across the nanoparticle and the role of surface patch charges is highly relevant for the interaction between dielectric particles and surfaces and will require further intense experimental study.

1. Competing optical effects

In principle, it seems possible that the emergence of the anharmonic trapping potential is due to an optical effect rather than being induced by dispersive surface interactions. A tiny fraction of light incident to the particle and surface is reflected by the surface in such a way that it reduces the laser power incident to the trap and therefore lowers the x^2 trapping potential. This effect is, however, separable from the effect of the surface interactions, as these scale as inverse powers of the distance from the surface and therefore are always asymmetric about the particle position, while the optical potential is composed of symmetric x^2 terms for the region of the trap explored by the particle. Further, when the purely optical potential dynamics is parametrically driven into its nonlinear regions as, for instance, for high oscillation amplitudes, x^4 and higher-order symmetric Duffing terms appear. This means that anharmonic terms, which would result in a nonsymmetric

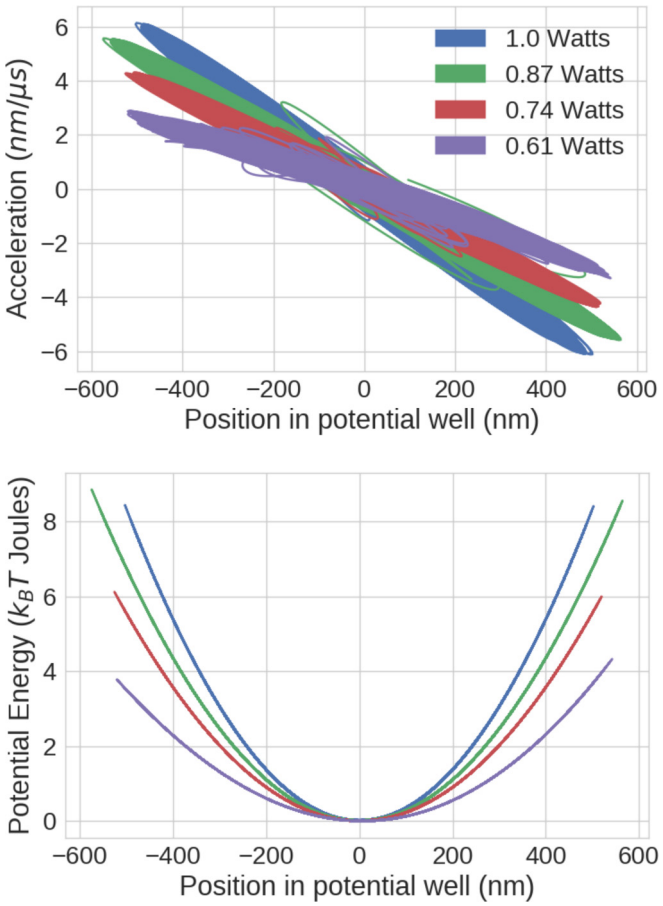

FIG. 7. Trapping laser power dependency of the spring function and trapping potential. Despite the change in laser power, the optical potential remains composed of x^2 and higher-order symmetrical terms. The spring function remains linear. Data have been taken for large distances between particle and surface.

potential, cannot be generated for a static optical potential in this geometry. Thus the anharmonic potential we observe cannot be explained by an optical effect.

We experimentally check the laser power dependence of the trap potential and observe that the potential as well as the spring functions remain of the x^2 and linear type, respectively (see Fig. 7). This further reinforces that the observed anharmonicity of the trapping potential for the particle close to the surface is not of optical origin.

Another effect may be caused by the multiple reflections of light between surface and particle, known as optical binding, which have a similar scaling with distance as some dispersion forces. We argue that such multiple reflections will change the laser power forming the trap and conclude, per the same rationale given above, that optical binding cannot explain the observed anharmonicity in these experiments.

2. Laser power dependence of the trapping potential

Studying the change in spring functions for a trapped particle with different trapping laser powers demonstrates that the change is always symmetric, as shown in Fig. 7. We conclude that the observed anharmonicity cannot be explained by a laser-power-dependent optical effect.

VI. CONCLUSION

In summary, we have presented an experiment where the surface-induced force on a levitated nanoparticle can be directly observed. The particle-surface interaction induces an anharmonic trapping potential in deviation from the harmonic (x^2) behavior and therefore generates a nonlinearity in the motion of the particle. This nonlinearity affects all trapped states, while the overall dynamics is still dominated by the linear term of the optomechanical harmonic oscillator. We associate the observed anharmonic effect with a particle-surface interaction involving electric charge. The current force sensitivity is three orders of magnitude too small at the particle-surface distances reached in order to allow for the detection of CP forces with a levitated nanoparticle. In future the experiment could be repeated with a particle with zero net, of a larger size, and closer to the surface to reach such smaller forces. The careful analysis of the particle position measured in the lateral directions along the surface may allow for topographic images in close analogy to scanning probe techniques. A further advantage of a levitated nanoparticle probe might be that the measurement can be performed with a very high precision, while both surface and nanoparticle are at room temperature. Subject to appropriate limitations concerning optical transparency of the sample, this could be interesting in the context of biological and physiological samples. As suggested recently, rotation of nonspherical nanoparticles close to surfaces might be another interesting system for investigation of surface forces [33]. This work may pave the way for cooling [34] and trapping of nanoparticles in vacuum close to surfaces in self-induced back-action-type near-field traps [35], invoking both plasmonic and photonic crystal effects to trap the particle. The described experiments may also be applied to study electric field noise effects and their physical origins [19].

ACKNOWLEDGMENTS

We would like to thank David Hempston, Marko Toroš, Chris Timberlake, and Ashley Setter for discussions. H.U., M.R., and G.W. acknowledge funding from The Leverhulme Trust, the EU Horizon 2020 FET project TEQ (Grant No. 766900), and the Foundational Questions Institute (FQXi). G.W. acknowledges the collaborative education and research cosupervision program between the University of Southampton and the Japan Advanced Institute of Science and Technology. M.R. would like to acknowledge funding from the Erasmus+ program of Österreichischer Austauschdienst and the Top-Stipendium exchange scholarship of the state of Lower Austria. R.B. and S.B. acknowledge funding from the German DFG (Grant No. BU1803/3-1), the Alexander von Humboldt Foundation, and the Freiburg Institute for Advanced Studies (FRIAS).

APPENDIX A: MORSE POTENTIAL BEHAVIOR

The acceleration broadening [cf. Fig. 6(a)] of the particle's motion close to the surface can be best understood in an energetic picture. The limitation on the closest approach to the surface is encountered when the surface potential overpowers the optical potential well. The overall potential of the system appears similar to a Morse potential, whose degree of

anharmonicity can be best understood by constructing a histogram of the particle's energy as its motion in the trap is sampled.

For the unperturbed case, the particle undergoes harmonic motion, which can then be used in the potential energy $U = \frac{1}{2}kx(t)^2$, and its equation of motion is simply $x(t) = x_0 \cos \omega t$. Making a histogram of the potential felt by the particle at evenly spaced times results in a two-peak shape, which can be explained by solving the equation of motion for t, which gives

$$t = \frac{1}{\omega} \arccos\left[\frac{1}{x_0}\sqrt{\frac{2U}{k}}\right]. \tag{A1}$$

The time spent within any time interval dt will then be given by

$$dt = \frac{dt}{dU}dU = -\frac{\mathrm{sgn}(x_0)}{\omega\sqrt{2U}\sqrt{kx_0^2 - 2U}}dU, \tag{A2}$$

which, subject to proper normalization, corresponds to the likelihood of the particle's being observed within a potential energy of between U and $U + dU$. It is clear that dt has maxima at $U = 0$ and $U = \frac{1}{2}kx_0^2$, resulting in the two-peak structure discussed above. However, this is not seen in the histogram of energies extracted from the experimental data (cf. Fig. 5); rather, a single peak at $U = 0$ is found in both the harmonic and the anharmonic cases.

This difference comes from the fact that the motion of the particle in the trap is not in fact well described by simple harmonic motion; the experiment takes place in a vacuum of 10^{-2} mb, meaning that the particle's motion is still affected by collisions with the background gas. We incorporate this into the description of the system by assuming that the motion may be taken to be averaged over many trajectories, each with a different amplitude x_0, Gaussian distributed about some mean value $\bar{x}_0$ with a standard deviation σ. Thus we calculate

$$\overline{dt} = -\frac{1}{\sqrt{2\pi\sigma^2}}\int_{\sqrt{2U/k}}^{\infty} dx_0 e^{(x_0-\bar{x}_0)^2/(2\sigma^2)} \times \frac{\mathrm{sgn}(x_0)}{\omega\sqrt{2U}\sqrt{kx_0^2 - 2U}}dU, \tag{A3}$$

with x_0 being the integration variable and σ being the only fitting parameter. The result for $\sigma = 100$ nm is shown in Fig. 5, alongside the experimental data and a numerical simulation for both harmonic and anharmonic potentials. In the latter case the equations of motion cannot be solved analytically, so there is no equivalent of Eq. (A3) for the anharmonic potential. It is seen that our modeling of the background gas collisions by smearing out the amplitude of the oscillations is consistent with experimental results, especially for a relatively high energy. All the results display the required behavior of having a single peak at $U = 0$, which can be intuitively understood from our averaging procedure; since all the trajectories pass through $U = 0$ many times but have different maximum values, the peak of Eq. (A2) at $U = \frac{1}{2}kx_0^2$ is suppressed.

APPENDIX B: CASIMIR-POLDER POTENTIAL

The CP potential $U(z)$ of a particle with polarizibility $\alpha(\omega)$ a distance z from a layer of thickness L and relative permittivity $\epsilon_1(\omega)$, supported by an infinitely deep substrate with relative permittivity $\epsilon_2(\omega)$, is given by [36]

$$U_{\mathrm{CP}}(z) = \frac{\hbar\mu_0}{8\pi^2}\int_0^\infty \xi^2\alpha(i\xi)\int_{\xi/c}^\infty d\kappa_0\, e^{-2\kappa_0 z}\Big[R_{\mathrm{TE}}(\kappa_0,\kappa_1,\kappa_2) + \left(1 - 2\frac{\kappa_0^2c^2}{\xi^2}\right)R_{\mathrm{TM}}(\kappa_0,\kappa_1\kappa_2)\Big] \tag{B1}$$

where, for either polarization σ (=TE, TM),

$$R_\sigma = \frac{R_{01}^\sigma + e^{-2\kappa_1 L}R_{12}^\sigma}{1 + e^{-2\kappa_1 L}R_{01}^\sigma R_{12}^\sigma}, \tag{B2}$$

with

$$R_{ij}^{\mathrm{TE}} = \frac{\kappa_i - \kappa_j}{\kappa_i + \kappa_j}, \quad R_{ij}^{\mathrm{TM}} = \frac{\epsilon_j(i\xi)\kappa_i - \epsilon_i(i\xi)\kappa_j}{\epsilon_j(i\xi)\kappa_i + \epsilon_i(i\xi)\kappa_j} \tag{B3}$$

and

$$\epsilon_0(i\xi) = 1, \quad \epsilon_1(i\xi) = \epsilon_{\mathrm{SiO_2}}(i\xi), \quad \epsilon_2(i\xi) = \epsilon_{\mathrm{Si}}(i\xi), \quad \kappa_i = \sqrt{[\epsilon_i(i\xi) - 1]\xi^2/c^2 + \kappa_0^2}. \tag{B4}$$

A small sphere of radius R may be modeled via the Clausius-Mossotti polarizability shown in Eq. (7). Using this relation, Eq. (B1) is now a formula whose inputs are the dielectric functions for the media that make up the substrate, layer, and sphere, which are all known from experiments. As discussed in the text, we eventually approximate this by its large-distance limit near a simple half-space of permittivity $\epsilon_1(\omega)$, in which case the potential takes the form

$$U_{\mathrm{CP}}(z) = -\frac{C_4}{z^4}, \tag{B5}$$

where C_4 is a distance-independent constant defined as [27]

$$C_4 = \frac{3\hbar c\alpha(0)}{64\pi^2\epsilon_0}\int_1^\infty dv\left(\frac{2}{v^2} - \frac{1}{v^4}\right)\frac{\epsilon_1(0)v - \sqrt{\epsilon_1(0) - 1 + v^2}}{\epsilon_1(0)v + \sqrt{\epsilon_1(0) - 1 + v^2}}. \tag{B6}$$

In the experiment presented in the text the surface is silicon and the sphere is silicon dioxide. We model both of these via an N-resonance Drude-Lorentz permittivity, defined by

$$\epsilon(\omega) = 1 + \sum_{i=1}^{N}\frac{\omega_{p,i}^2}{\omega_{T,i}^2 - \omega^2 + i\gamma_i\omega}. \tag{B7}$$

Here $\omega_{p,i}$ is the plasma frequency, $\omega_{T,i}$ is the transition frequency, and γ_i is the damping frequency, each for the ith resonance of the dielectric function. For silicon we use a single-resonance model, and for silicon dioxide we use a two-resonance model, with parameters from [26] listed in Table I. Using these parameters in Eq. (B6) we find the dispersion constant C_4 for our particular setup:

$$C_4 = (7.60 \times 10^{-28}\ \mathrm{J \cdot m})R^3. \tag{B8}$$

As a consistency check we evaluate Eq. (B1) numerically over both distance regimes; the results of this alongside the

TABLE I. Drude-Lorentz parameters for silicon and silicon dioxide (all values in units of 10^{15} rad/s).

	i	$\omega_{p,i}$	$\omega_{T,i}$	γ_i
Si	1	23	7.1	0.98
SiO_2	1	0.17	0.13	0.043
	2	29	27	8.1

asymptotic long-distance result according to Eq. (B8) are shown in Fig. 8 for a range of sphere sizes.

APPENDIX C: FORCE SENSITIVITY

The particle position is measured in volts at the detector. By fitting to the PSD (which has units of $V/\sqrt{Hz}$) we can extract a conversion factor, γ_c, which is in units of volts per meter (V/m). From here, we can convert all our measurements to meters. Although the Lorentzian fitting has small errors (typically <1%.), the error in the conversion factor is substantially higher due to the 15% error in our pressure reading. Specifically, we calculate the mass from knowledge of the fitting to the Lorentzian and the pressure. Thus, the error propagates into our conversion factor through the error in the mass (for further details see [22]). The conversion factor is given by

$$\gamma_c = \sqrt{\frac{A}{C}\frac{\pi m}{kBT_0}}, \tag{C1}$$

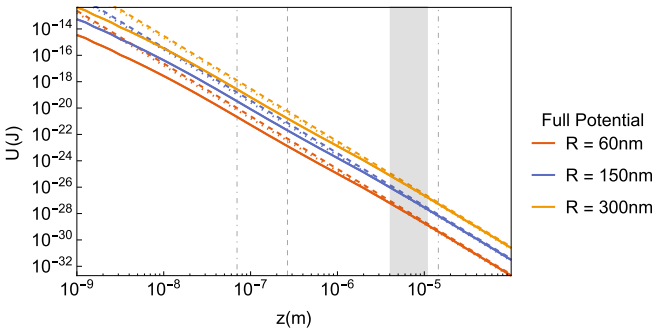

FIG. 8. Casimir-Polder potential of SiO_2 spheres of various radii near a Si plate. Solid curves are exact results found from numerical integration of (B1), while dotted curves are from the approximate form Eq. (B6). We also show with dashed lines the result of evaluating Eq. (B6) using instead the permittivity of Si for the half-space. The absorption wavelengths of the two media involved are shown as vertical lines (dashed for silicon, dot-dashed for silicon dioxide), while the experimental region of interest (~4 to 11 μm) is shaded gray. It is shown that this experiment is taking place at distances larger than the dominant transition wavelengths of either medium involved (the longer-wavelength silicon dioxide transition is significantly weaker than the shorter-wavelength one, corresponding to a much smaller value of ω_p in Table I). Both half-space approximations agree well with the full numerical integration of the layered potential, but in Fig. 9 it is shown that closer agreement is found with the silicon dioxide version.

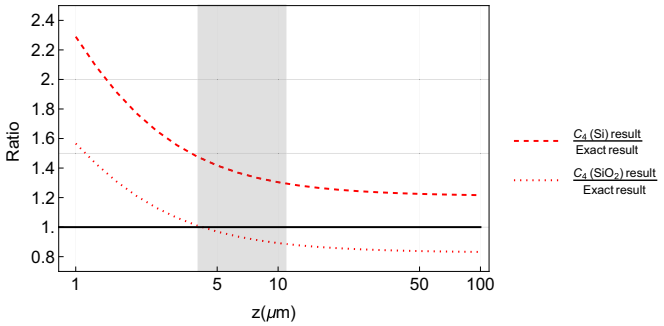

FIG. 9. Ratio of the approximations shown in Fig. 8 to the exact numerical result (which is independent of the radius of the sphere). The silicon dioxide result is shown to agree well within the experimental region of interest.

where A is the amplitude of the fitted Lorentzian and C the width, m is the mass of the particle, and T_0 is the environmental gas temperature, assumed to be 300 K.

Therefore, the error in γ_c can be obtained from

$$\Delta\gamma_c = \gamma_c\sqrt{(\Delta A/A)^2 + (\Delta m/m)^2 + (\Delta C/C)^2}. \tag{C2}$$

This is of the order of ~34%. Position sensitivity, δx, is defined as the smallest positional change we can observe in our system, limited by the most dominant noise source, which manifests itself in the PSD noise floor. We therefore, extract the position sensitivity, and its error, from this noise floor, converting from volts to meters, to signify the smallest detectable signal from the motion of the particle to be

$$\delta x = \mathrm{PSD}_{\text{noise floor}}/\gamma_c, \tag{C3}$$

$$\Delta(\delta x) = \delta x\sqrt{\left(\frac{\Delta(\mathrm{PSD}_{\text{noisefloor}})}{\mathrm{PSD}_{\text{noisefloor}}}\right)^2 + (\Delta\gamma_c/\gamma_c)^2}. \tag{C4}$$

For our experimental parameters this is 1 ± 0.4 nm/$\sqrt{Hz}$. The force sensitivity can be obtained from

$$\delta F = \frac{1}{2}m\omega_0^2\delta x, \tag{C5}$$

$$\Delta(\delta F) = \delta F\sqrt{(\Delta m/m)^2 + (\Delta(\delta x)/\delta x)^2}, \tag{C6}$$

where ω_0 is the oscillator frequency and we have assumed the error in the oscillator frequency to be negligible. Hence, our force sensitivity for the current experiments is $8 \pm 3 \times 10^{-17}$ N/$\sqrt{Hz}$. This can be substantially improved upon if we improve the signal-to-noise ratio of our signal, as was the case in previous work [37], where the force sensitivity was as low as 10^{-19} N/$\sqrt{Hz}$ [29]. In this case, a higher signal-to-noise ratio gives rise to a higher position sensitivity in addition to resonant driving.

[1] S.-W. Lee and W. M. Sigmund, J. Colloid Interface Sci. **243**, 365 (2001).

[2] R. H. French, V. A. Parsegian, R. Podgornik, R. F. Rajter, A. Jagota, J. Luo, D. Asthagiri, M. K. Chaudhury, Y.-m. Chiang, S. Granick, S. Kalinin, M. Kardar, R. Kjellander, D. C. Langreth, J. Lewis, S. Lustig, D. Wesolowski, J. S. Wettlaufer, W.-Y. Ching, M. Finnis, F. Houlihan, O. A. von Lilienfeld, C. J. van Oss, and T. Zemb, Rev. Mod. Phys. **82**, 1887 (2010).

[3] A. A. Geraci, S. B. Papp, and J. Kitching, Phys. Rev. Lett. **105**, 101101 (2010).

[4] K. A. Dill, Biochemistry **29**, 7133 (1990).

[5] A. Nicholls, K. A. Sharp, and B. Honig, Proteins: Struct. Funct. Bioinfo. **11**, 281 (1991).

[6] L. Yang, C. Adam, G. S. Nichol, and S. L. Cockroft, Nat. Chem. **5**, 1006 (2013).

[7] D. J. Kapner, T. S. Cook, E. G. Adelberger, J. H. Gundlach, B. R. Heckel, C. D. Hoyle, and H. E. Swanson, Phys. Rev. Lett. **98**, 021101 (2007).

[8] D. C. Moore, A. D. Rider, and G. Gratta, Phys. Rev. Lett. **113**, 251801 (2014).

[9] J. Schmöle, M. Dragosits, H. Hepach, and M. Aspelmeyer, Class. Quantum Gravity **33**, 125031 (2016).

[10] P. Hamilton, M. Jaffe, P. Haslinger, Q. Simmons, H. Müller, and J. Khoury, Science **349**, 849 (2015).

[11] H. B. G. Casimir, Proc. K. Ned. Akad. Wet. **51**, 793 (1948).

[12] H. B. G. Casimir and D. Polder, Phys. Rev. **73**, 360 (1948).

[13] S. K. Lamoreaux, Phys. Rev. Lett. **78**, 5 (1997).

[14] U. Mohideen and A. Roy, Phys. Rev. Lett. **81**, 4549 (1998).

[15] A. Shih and V. A. Parsegian, Phys. Rev. A **12**, 835 (1975).

[16] C. I. Sukenik, M. G. Boshier, D. Cho, V. Sandoghdar, and E. A. Hinds, Phys. Rev. Lett. **70**, 560 (1993).

[17] J. M. Obrecht, R. J. Wild, M. Antezza, L. P. Pitaevskii, S. Stringari, and E. A. Cornell, Phys. Rev. Lett. **98**, 063201 (2007).

[18] H. Bender, C. Stehle, C. Zimmermann, S. Slama, J. Fiedler, S. Scheel, S. Y. Buhmann, and V. N. Marachevsky, Phys. Rev. X **4**, 011029 (2014).

[19] M. Brownnutt, M. Kumph, P. Rabl, and R. Blatt, Rev. Mod. Phys. **87**, 1419 (2015).

[20] G. Binnig, C. F. Quate, and C. Gerber, Phys. Rev. Lett. **56**, 930 (1986).

[21] M. Rashid, T. Tufarelli, J. Bateman, J. Vovrosh, D. Hempston, M. S. Kim, and H. Ulbricht, Phys. Rev. Lett. **117**, 273601 (2016).

[22] J. Vovrosh, M. Rashid, D. Hempston, J. Bateman, M. Paternostro, and H. Ulbricht, JOSA B **34**, 1421 (2017).

[23] J. Steinlechner, C. Krüger, N. Lastzka, S. Steinlechner, A. Khalaidovski, and R. Schnabel, Class. Quantum Gravity **30**, 095007 (2013).

[24] L. Rondin, J. Gieseler, F. Ricci, R. Quidant, C. Dellago, and L. Novotny, Nat. Nanotechnol. **12**, 1130 (2017).

[25] P. Barcellona, R. Bennett, and S. Y. Buhmann, J. Phys. Commun. **2**, 035027 (2018).

[26] E. D. Palik, *Handbook of Optical Constants of Solids* (Academic Press, New York, 1985).

[27] L. Spruch and Y. Tikochinsky, Phys. Rev. A **48**, 4213 (1993).

[28] M. Frimmer, K. Luszcz, S. Ferreiro, V. Jain, E. Hebestreit, and L. Novotny, Phys. Rev. A **95**, 061801 (2017).

[29] D. Hempston, J. Vovrosh, M. Toroš, G. Winstone, M. Rashid, and H. Ulbricht, Appl. Phys. Lett. **111**, 133111 (2017).

[30] A. Sushkov, W. Kim, D. Dalvit, and S. Lamoreaux, Nat. Phys. **7**, 230 (2011).

[31] R. O. Behunin, Y. Zeng, D. A. R. Dalvit, and S. Reynaud, Phys. Rev. A **86**, 052509 (2012).

[32] A. Derevianko, W. R. Johnson, M. S. Safronova, and J. F. Babb, Phys. Rev. Lett. **82**, 3589 (1999).

[33] A. Manjavacas, F. J. Rodríguez-Fortuño, F. J. García de Abajo, and A. V. Zayats, Phys. Rev. Lett. **118**, 133605 (2017).

[34] R. Diehl, E. Hebestreit, R. Reimann, F. Tebbenjohanns, M. Frimmer, and L. Novotny, Phys. Rev. A **98**, 013851 (2018).

[35] M. L. Juan, R. Gordon, Y. Pang, F. Eftekhari, and R. Quidant, Nat. Phys. **5**, 915 (2009).

[36] I. Dzyaloshinskii, E. Lifshitz, and L. Pitaevskii, Adv. Phys. **10**, 165 (1961).

[37] M. Rashid, M. Toroš, and H. Ulbricht, Quant. Meas. Quant Met. **4**, 17 (2017).